Received: 6 May 2023 | Revised: 27 August 2023 | Accepted: 2 September 2023

IET Microwaves, Antennas & Propagation

DOI: 10.1049/mia2.12420

The Institution of Engineering and Technology WILEY

ORIGINAL RESEARCH

A two-dimensional beam steering Fabry–Pérot antenna employing a liquid-based reconfigurable metasurface

Wei Chen[1] | **Zhiming Liu**[1] | **Huilin Zhou**[1] | **Jens Bornemann**[2] | **Yuhao Wang**[1] | **Fei Wang**[3]

[1]Nanchang University, School of Information Engineering, Nanchang, China

[2]Department of Electrical and Computer Engineering, University of Victoria, Victoria, British Columbia, Canada

[3]Fujian Key Laboratory of Special Energy Manufacturing, Huaqiao University, Xiamen, China

Correspondence

Zhiming Liu, Nanchang University, School of Information Engineering, Nanchang 330031, China.
Email: zhimingliu@ncu.edu.cn

Funding information

Jiangxi Provincial Natural Science Foundation, Grant/Award Number: 20224BAB212005; Open Fund of the key laboratory of radar imaging and microwave photon technology of the Ministry of Education, Grant/Award Number: NJ20220005; National Natural Science Foundation of China, Grant/Award Numbers: 62161027, 62201240

Abstract

A novel 2-D beam steering technology using a Fabry–Pérot antenna with a liquid-based reconfigurable metasurface is presented. The antenna employs a reconfigurable partially reflecting surface to regulate phase distribution and adopts a microstrip antenna as feed to realise 2-D beam steering. The antenna beam can be tilted in four different directions by injecting liquid metal into the specific area of the microfluidic channels embedded in the metasurface. Moreover, the antenna has a simple and compact structure with a low profile. A prototype is manufactured, and good agreement between simulated and experimental results verifies the correctness of the design. The measured results of the manufactured antenna prototype demonstrate that the main beam tilts to maximum values of ±15° and ±28° in the *yoz* and *xoz* planes, respectively, between 9.5 and 9.7 GHz.

KEYWORDS

antenna radiation patterns, beam steering, Fabry-Perot resonators, metamaterial antennas

1 | INTRODUCTION

Since Fabry–Pérot (FP) resonator theory was first applied in antennas in 1956 [1], the FP antenna, a high-gain antenna with simple and compact structure and without complex feed network, has been widely used in wireless communication systems [2–4]. Generally, a FP antenna is composed of a partially reflecting surface (PRS) and a source antenna. The PRS is placed parallel above the feed to form an FP resonant cavity with the ground embedded with the feed. After multiple reflections and transmissions, electromagnetic waves are superimposed in phase outside the cavity, thus the directivity of radiating sources at boresight is enhanced. However, its high Q factor will cause the radiation bandwidth of the antenna to decrease [5]. Reconfigurable antennas are multifunctional and highly integrated antennas, which can improve the channel capacity [6, 7], expand the signal radiation range [8] and reduce the coupling between antenna elements [9].

Usually, there are two methods to realise beam steering: (i) using a phased array as the feed antenna [10, 11] and (ii) employing a PRS with adjustable reflection phase [12–16]. The first method can effectively adjust the radiation beam by controlling the excitation unit of the phased array. However, this method does not conform to the development trend of antenna simplification due to electromagnetic coupling and the design of the feed network. For the second method, the phase distributions of PRSs are changed by controlling the on–off states of microwave switching elements [12–14] and introducing metasurfaces with phase modulation characteristics [15, 16], which require an additional bias circuit in general.

In this paper, a novel technology is proposed to realise radiation pattern reconfigurability. In the proposed antenna,

the liquid-based reconfigurable metasurface (LRMS) composed of agile array reflection phase units is employed as PRS and forms a FP resonant cavity with the feed. Different phase defects are obtained by injecting liquid metal eutectic gallium indium (EGaIn) into specific areas in the LRMS. Under the excitation of microstrip patch antenna, different phase defects lead to corresponding beam inclination and angle. Thus, the antenna can achieve 2-D beam steering, and the experiments of the processed prototype verifies that its main beam is tilted about ±15° and ±28° in *yoz* and *xoz* planes at 9.5–9.7 GHz, respectively. With respect to introducing multi-phase defects into the PRS structure, the proposed reconfigurable method is simpler and has lower design complexity compared with phased array and electric control methods [10–14]. Also, the antenna designed by this method can avoid electromagnetic interference caused by the circuit because it does not require additional biasing networks. Particularly, compared with the liquid-based reconfigurable method similar to Ref. [17], the proposed method achieves 2-D pattern reconfigurability with larger and almost constant beam steering angles over a relatively wide frequency range instead of 1-D beam tilting at a single frequency. In summary, the proposed design achieves good radiation performance with a simple and compact structure, and is suitable for complex operational environments without requiring additional bias circuits. It may have potential applications in the wireless communication fields.

2 | DESIGN STRATEGY OF RECONFIGURABLE LIQUID-BASED RECONFIGURABLE METASURFACE

Liquid metal EGaIn can be applied in the design of reconfigurable antennas because of its high conductivity (3.4×10^6 S/m) and stable physical properties [17–19]. A 3D view of the unit cell of the LRMS is shown in Figure 1. It consists of three dielectric layers, all of which are made of F_4B material (Wangling, Taizhou, Jiangsu and CHN) with a tanδ of 0.001, and a square metal patch printed on the bottom layer. A microfluidic channel with a thickness of 0.8 mm is embedded in the middle layer and can be injected with EGaIn. The thicknesses of the bottom layer (F4BK265 substrate, $\varepsilon_r = 2.65$), the middle layer (F4BK300 substrate, $\varepsilon_r = 3$) and the top layer (F4BK350 substrate, $\varepsilon_r = 3.5$) are 1.5 mm, 0.8 and 2 mm, respectively.

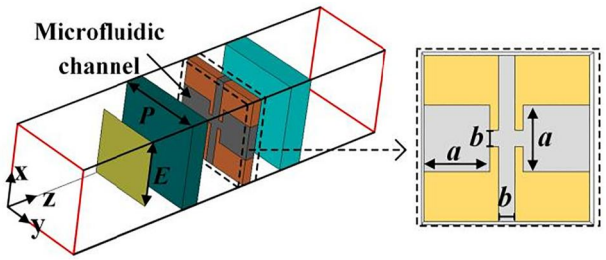

FIGURE 1 3D view of unit cell structure for regulating liquid-based reconfigurable metasurface (LRMS) phase distribution. Parameters: p = 7.1 mm, E = 5.4 mm, a = 2.84 mm, b = 0.7 mm.

According to the ray tracing model, the maximum directivity is obtained when the FP antenna satisfies the following Equation [1]

$$H = \frac{\lambda_0}{4\pi}(\phi_1 + \phi_2) + \frac{\lambda_0}{2}n,\ n = 0, 1, 2... \quad (1)$$

where H represents the distance between the PRS and ground, and λ_0 is the wavelength in free space. φ_1 and φ_2 refer to the reflection phases of the PRS and ground plane, respectively. Since a total reflection ground is adopted, $\varphi_2 = \pi$; so when the operating frequency is determined, H is only related to φ_1. To reduce the height of the FP cavity, the reflection phase of the unit cell containing EGaIn at the operating frequency (10 GHz) is adjusted to about zero; then H according to (1) equals to a quarter of λ_0.

The LRMS is composed of 10 × 10 periodic unit cells with uneven phase distribution and is designed for operation at 10 GHz. It is common knowledge that FP antenna employing PRS with uniform phase distribution will radiate a broadside beam, and introducing a progressive phase shift in PRS can realise beam tilt. Figure 2 3D view and side view of unit cell with more details, the shape of that microfluidic channel and its position in the unit cell are highlighted. By injecting and extracting EGaIn in the microfluidic channel, the unit cell can obtain two different reflection phases and magnitudes. Based on that, the approach proposed in this paper is to achieve the phase distribution regulation of LRMS by injecting EGaIn into its specific areas, so as to realise beam steering. From Figure 3,

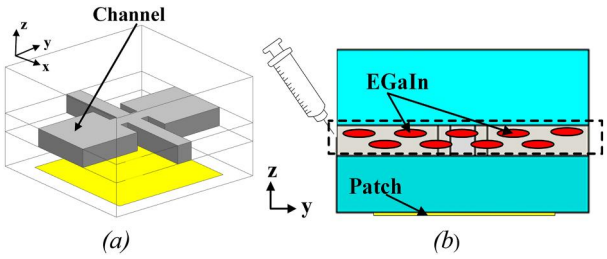

FIGURE 2 3D view (channel and patch are highlighted) and side view of unit cell; (a) 3D view; (b) side view.

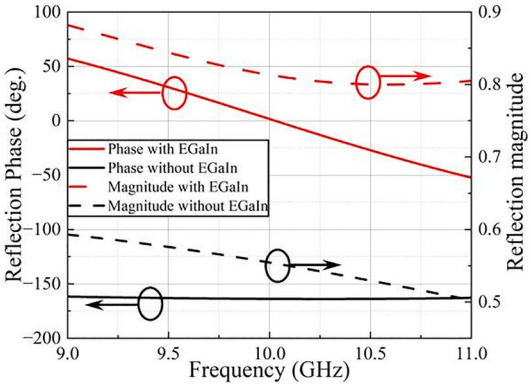

FIGURE 3 Simulated reflection phase and magnitude of the unit cell with/without EGaIn.

it can be observed that when the microfluidic channel is injected with EGaIn, the reflection phase and magnitude of the unit cell are 0 and 0.81, respectively; and when the EGaIn is extracted, its reflection phase and magnitude decrease to −163° and 0.55. Apparently, comparing the two states of the unit cell, the reflection phase tends to be constant in the frequency band between 9 and 11 GHz when the EGaIn is extracted, which lags behind that when the EGaIn is injected, and the magnitude decreases. The primary factor that contributes to this situation is the fact that the air cavity in the microfluidic channels has little impact on the phase and the reflection of electromagnetic waves.

With respect to the feed, a simple microstrip patch antenna fed by a single coaxial probe operating at 10 GHz is employed as excitation. The feed antenna shows a good impedance match ($|S_{11}| < -10$ dB) from 9.73 to 10.23 GHz (5.0%).

3 | DESIGN AND PERFORMANCE ANALYSIS OF ANTENNA

The configuration of the proposed FP antenna is shown in Figure 4, which is composed of the feed antenna and the LRMS. The driven patch is printed on the F_4B substrate ($\tan\delta = 0.0007$, $\varepsilon_r = 2.65$) with a thickness of 1 mm. The ground of the feed antenna forms a resonant cavity with the PRS placed parallel to it at a distance H. According to (1), the FP antenna is expected to be designed to resonate at 10 GHz with a height of $H = 7.5$ mm. However, due to the more intense electromagnetic coupling caused by the reduction of the height, the resonance frequency is offset to 9.6 GHz, and the height of the cavity H is optimised to 7.9 mm. Each unit cell of LRMS is considered as an element of phased array. The proposed LRMS appears uneven phase distribution due to the injection of EGaIn in the specific areas. The main beam of the antenna will tilt to the phase lag part of LRMS. Therefore, the direction of beam tilt can be controlled by phase distribution regulation of LRMS, which is realised by injection of EGaIn. For the angle of the main beam of the antenna θ, it satisfies the following expression [20]:

$$\sin\theta = \frac{\beta}{k_0} \tag{2}$$

where β is the phase constant of the leaky wave antenna and k_0 is the free space wavenumber.

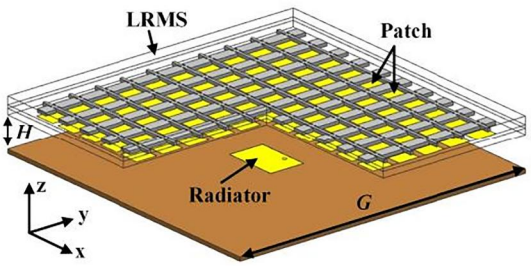

FIGURE 4 Configuration of the proposed Fabry–Pérot (FP) antenna. Parameters: $G = 78$ mm, $H = 7.9$ mm.

When the microfluidic channels of the LRMS are completely filled with EGaIn, it is regarded as the Original State. As a result of the bottom patch of the LRMS and the injected EGaIn, the antenna resonates at two additional frequency points, which leads to a wider bandwidth. Its 10-dB return loss bandwidth stretches from 9.50 to 10.79 GHz (12.7%). Other states (State 1 and State 3) occur when the unit cells in the first and second columns, respectively, near the centre of the $-y$ direction are extracted from EGaIn. For State 1 and State 3 of the antenna, the air cavity in the microfluidic channel will make its phase lag behind the LRMS on the other side, which will cause the main beam to tilt in the $-y$ direction. Figure 5 depicts more intuitively the states corresponding to different filling areas of EGaIn. Similarly, the main beam of the antenna will tilt to the $-x$ direction in State 6 and State 8. Furthermore, in Figure 5, the areas of extracted EGaIn symmetrical to States 1, 3, 5 and 7 are marked with black boxes, which are called States 2, 4, 6 and 8, respectively.

It is necessary to analyse the phase distribution of the antenna. Figure 6 shows the simulated phase distribution of the FP antenna in different states on observation plane with a height of 5 mm above LRMS. The phase change of antenna edge due to the edge effect of LRMS is not considered. As can be seen from Figure 6, in the Original State, the phase distribution in the central area of the antenna is uniform, which leads to a broadside beam. In the marked area, compared with the $+y$ direction, the antenna in State 1 has a phase lag of about 100° in the $-y$ direction, which leads to the beam tilting to the $-y$ direction. Liquid-based reconfigurable metasurface has obvious phase lag in the area of $+y$ direction in State 4, so

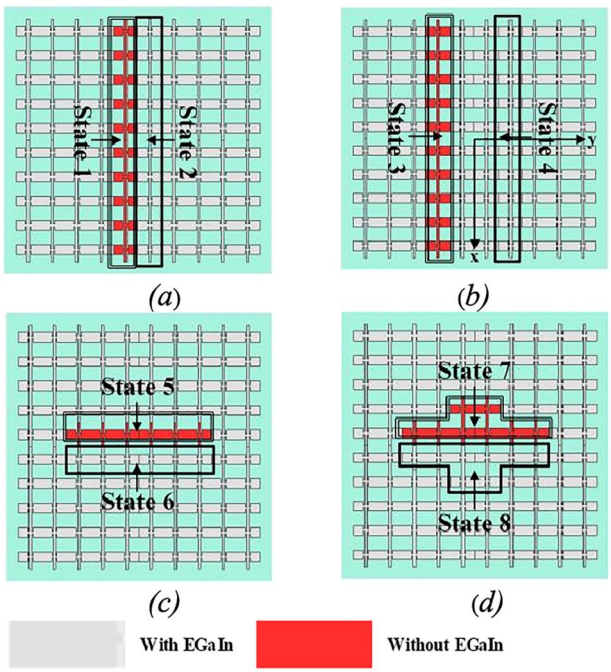

FIGURE 5 Corresponding states of filling areas with EGaIn. (a) State 1 and State 2; (b) State 3 and State 4; (c) State 5 and State 6; (d) State 7 and State 8.

the beam tilts in $+y$ direction. For similar reasons, the antenna beam tilts to $-x$ direction and $+x$ direction in State 5 and State 8, respectively.

The simulated realised gain patterns at 9.5 GHz, 9.6 and 9.7 GHz are shown in Figure 7, the angle of the beam tilted at the maximum realised gain is also indicated. Due to the symmetry of the LRMS structure, the beam radiates in the normal direction in the Original State. Also, compared with States 1, 3, 5 and 7, the antenna beams in States 2, 4, 6 and 8 are steered to the opposite direction with similar maximum realised gain at the same frequency. In States 1–4, the antenna beams with maximum realised gain at 9.5 GHz, 9.6 and 9.7 GHz are tilted to ±16° and ±10°, ±16° and ±8° and ±15° and ±7° of the *yoz* plane. Analogously, the simulated maximum realised gain appears at ±26° and ±19°, ±26° and ±18° and ±28° and ±15° of the *xoz* plane. Generally, as the antenna acquires the beam tilt property, its maximum realised gain will be slightly lower due to the significant changes of reflection amplitude and phase of unit cells. Also, when the beams of the antenna turn to the x-axis direction, the antenna shows lower realised gains compared with those turning to the y-axis direction. The essential reason is that the polarisation direction of the proposed antenna tends to the y-axis direction, and as the LRMS structure changes in y-direction, the current path changes more obviously and leads to a larger phase shift.

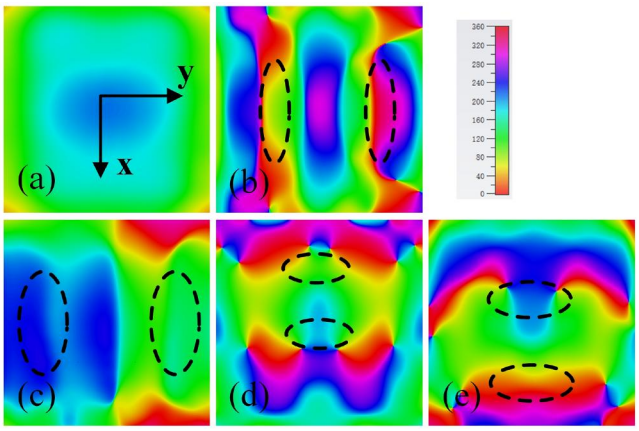

FIGURE 6 Simulated phase distribution of the proposed antenna in different States at 9.6GHz. (a) Original State; (b) State 1; (c) State 4; (d) State 5; (e) State 8.

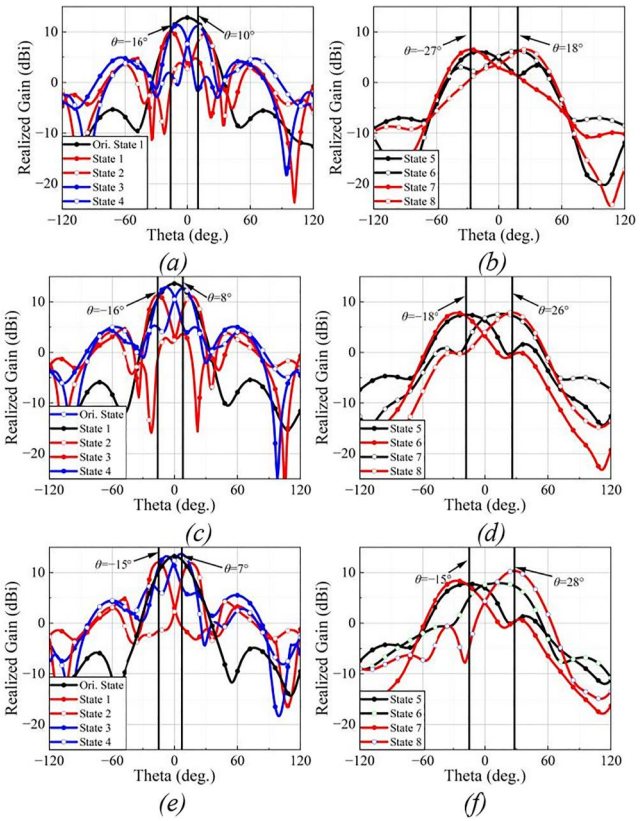

FIGURE 7 Simulated radiation patterns of the proposed antenna in different States. (a) 9.5 GHz, *yoz* plane; (b) 9.5 GHz, *xoz* plane; (c) 9.6 GHz, *yoz* plane; (d) 9.6 GHz, *xoz* plane; (e) 9.7 GHz, *yoz* plane; (f) 9.7 GHz, *xoz* plane.

The proposed antenna can realise beam steering from 9.5 to 9.7 GHz. The simulated beam directions and gains are shown in Table 1. For the sake of brevity, the simulated results are shown in only five states that represent the antenna performance. In each state in the frequency band of 9.5–9.7 GHz, the realised gain differs to varying degrees which is attributed to the difference in impedance matching.

In the aspect of antenna efficiency, after introducing LRMS above the feed, the simulated total radiation efficiency of the antenna at operating frequency centre (9.6 GHz) is enhanced from 76% to 90%, which shows that the resonant cavity composed of feed and LRMS improves the radiation efficiency of the antenna. In addition, the aperture efficiency of the antenna at 9.6 GHz is 24%, the insertion loss is 3.3 dB and the insertion phase shift is 26.1°. Generally speaking, the antenna has good radiation efficiency, and the reason for relatively low aperture efficiency is related to the low aperture efficiency of the microstrip patch antenna itself.

4 | EXPERIMENTAL RESULTS

In order to verify the numerical results of Section 2 and Section 3, a prototype of the proposed antenna has been fabricated and measured. Figure 8 shows photographs of the fabricated antenna and the structure of its middle layer. As shown in Figure 8a, the

TABLE 1 Simulated radiation performance of the proposed antenna.

State *Fr.*/GHz		Ori.	1	4	5	8
Max. Gain (dBi)	9.5	12.8	10.1	11.2	6.1	6.6
	9.6	13.6	11.4	12.7	7.5	7.9
	9.7	13.2	12.0	13.7	7.8	10.3
Beam direction (deg.)	9.5	0	16 (−*y*)	10 (+*y*)	19 (−*x*)	25 (+*x*)
	9.6	0	16 (−*y*)	8 (+*y*)	18 (−*x*)	26 (+*x*)
	9.7	0	15 (−*y*)	7 (+*y*)	15 (−*x*)	28 (+*x*)

four corners of the feed antenna and the PRS are drilled with holes to support them with spliced M2.5 nylon bolts. Four round holes at the edge of the top layer of LRMS are dug through to connect the channels of the middle layer for the injection of liquid metal. The positions of the liquid metal injection sites and more details of the microfluidic channels are depicted in Figures 8b,c respectively. In the experiment, liquid metal was injected into the microfluidic channels of LRMS by connecting silicone hoses with syringe, in order to fill the liquid metal into the specific area of the microfluidic channel smoothly; the foam, processed into the shape of the area where the liquid metal is not injected, is used to replace the air cavity to prevent it from flowing in. In addition, after extracting the EGaIn, we inject hydrochloric acid (0.365 wt %) to remove the EGaIn and its oxide that may remain in the channels. The liquid metal was injected manually through a syringe in the experiment, the method that is less able to accurately control the pressure of the injection and the position of the liquid metal. A possible solution to this problem is the use of microactuators for fine-tuning and positioning of the liquid metal.

The reflection coefficients are measured by a ZNB20 vector network analyser. The radiation patterns in the states that represent the antenna performance were measured in the far-field region in an anechoic chamber. The simulated and measured reflection coefficients of the proposed antenna in the Original State and feed are compared in Figure 9 and demonstrate very good agreement. After placing the LRMS in parallel above the feed, the change in the reflection characteristics of the antenna results in a shift in the current distribution, causing a deviation in the resonant frequency and the emergence of additional resonant peaks from different excitation modes, thereby expanding the bandwidth of the antenna. Figure 10 shows the simulated and measured results of

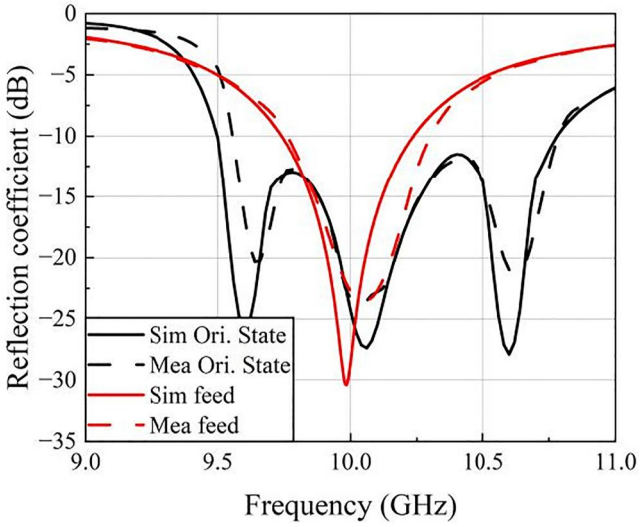

FIGURE 9 Simulated and measured reflection coefficients of the proposed antenna in Original State and feed.

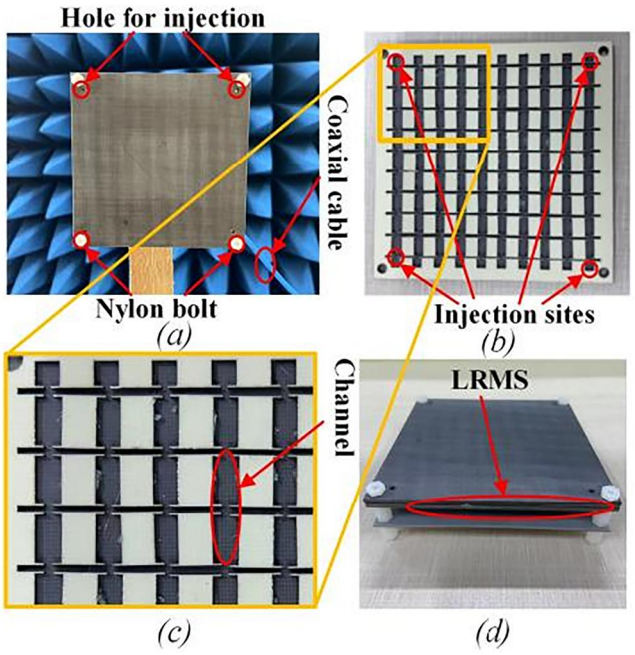

FIGURE 8 Photographs of the fabricated antenna prototype. (a) the antenna under test; (b) microfluidic channels embedded in the middle layer of PRS; (c) further details of the channel; (d) fabricated sample of the Fabry–Pérot (FP) antenna.

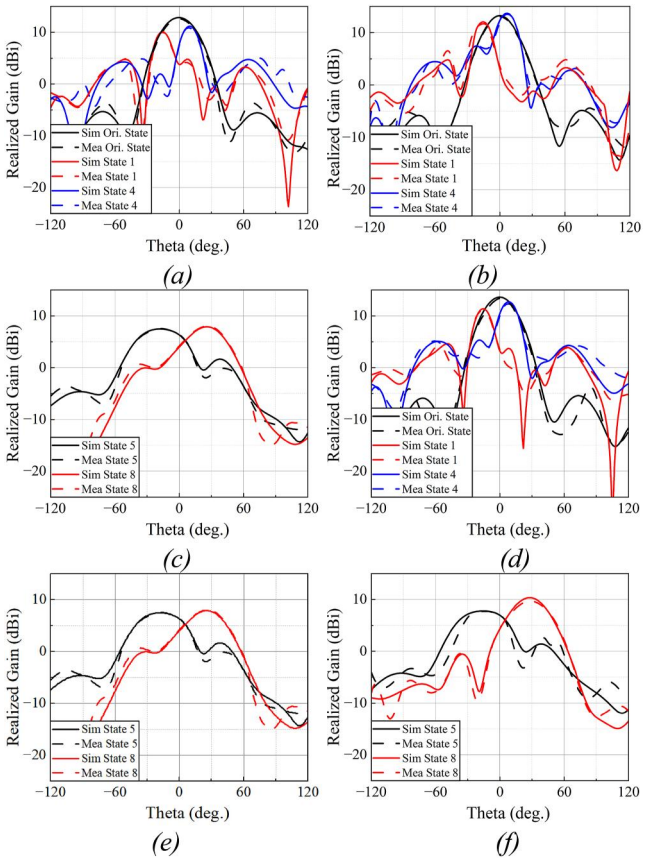

FIGURE 10 Radiation patterns of the proposed Fabry–Pérot (FP) antenna in different states. (a) 9.5 GHz, *yoz* plane; (b) 9.5 GHz, *xoz* plane; (c) 9.6 GHz, *yoz* plane; (d) 9.6 GHz, *xoz* plane; (e) 9.7 GHz, *yoz* plane; (f) 9.7 GHz, *xoz* plane.

TABLE 2 Comparison between the proposed antenna and existing works.

Ref.	Freq (GHz)	Aperture × H (λ_o^3)	RE (%)	Tilt direction	Technology	Beam tilt (°)
[12]	5.3–5.7	3.12 × 3.12 × 0.55	NA	1-D	PIN diodes	(y) ±4, ±6, ±9, ±15
[13]	5.6	5.00 × 5.00 × 0.47	NA	1-D	Varactor diodes	(y) 9–30
[14]	5.5	1.83 × 1.83 × 0.51	77	2-D	PIN diodes	(x, y) ±10
[17]	5.1	1.63 × 1.63 × 0.49	45–72	1-D	Liquid metal	(y) ±6, ±20
This work	9.5–9.7	2.50 × 2.50 × 0.25	90	2-D	Liquid metal	(x) ±15, ±27
						(y) ±8, ±15

Note: H represents the distance between the PRS and ground, RE denotes the radiation efficiency.

the antenna's main beam direction and its realised gain in four states at 9.5, 9.6 and 9.7 GHz. The measured realised gain of the antenna in the Original State is 12.6, 13.3 and 12.9 dBi at 9.5, 9.6 and 9.7 GHz, respectively. For State 1 and State 4, at 9.5, 9.6 and 9.7 GHz, the measured results show that the main beam of the antenna is tilted towards −16° and 8°, −16° and 7° and −15° and 6° of the *yoz* plane, respectively, and the corresponding realised gains are 10.0 dBi and 10.8 dBi, 11.1 dBi and 12.3 dBi and 11.2 dBi and 13.3 dBi, respectively. The measured realised gains of the antenna at 9.5, 9.6, and 9.7 GHz in states 5 and 8 are 5.9 dBi and 6.6 dBi, 7.5 dBi and 8.0 dBi and 7.7 dBi and 9.8 dBi, respectively, and the main beam is tilted at −18° and 25°, −17° and 26°, −15° and 28° in *xoz* plane. Some fine distinctions between experiment and simulation are mostly attributed to errors caused by manufacturing and the air gap remaining in the channel after being filled with liquid metal.

In Table 2, some physical and radiation characteristics of the proposed design are compared with existing works. The method of introducing varactors and PIN diodes in Refs. [12–14] requires additional feed networks, which increases design complexity and causes coupling between structures. Compared with Ref. [17], our proposed antenna realises 2-D beam steering and wider beam tilt range. We note that the proposed antenna has a lower profile. Moreover, the proposed antenna radiates broadside beams with better total radiation efficiency at the centre of the operating frequency.

5 | CONCLUSION

A new technology of a FP antenna with radiation pattern reconfigurability is proposed. The reflection phase of the LRMS can be changed by injecting liquid metal into specific channels. In the listed nine injection states, the main beam of the antenna is steered to an average range of 0°, ±8°, ±15° and ±15°, ±27° in the *yoz* and *xoz* planes, respectively, from 9.5 to 9.7 GHz. This work has positive implications for improving existing antenna technology and realisation of wider beam steering ranges in the future. The fact that a complex feed network is not required leads to a simple structure employing only a single feed for the antenna. In addition, the structure's low profile makes it attractive for applications in miniaturised and highly integrated antennas.

AUTHOR CONTRIBUTIONS

Wei Chen: Data curation; validation; writing – original draft. **Zhiming Liu**: Investigation; project administration; resources; supervision; writing – review & editing. **Huilin Zhou**: Methodology; supervision; writing – review & editing. **Jens Bornemann**: Formal analysis; supervision; writing – review & editing. **Yuhao Wang**: Resources; supervision; writing – review & editing. **Fei Wang**: Resources; validation.

ACKNOWLEDGEMENTS

National Natural Science Foundation of China, Grant/Award Number: 62201240, 62161027; Open Fund of the key laboratory of radar imaging and microwave photon technology of the Ministry of Education, Grant/Award Number: NJ20220005; Jiangxi Provincial Natural Science Foundation, Grant/Award Number: 20224BAB212005.

CONFLICT OF INTEREST STATEMENT

No co-authors have any conflicts of interest that need to be disclosed.

DATA AVAILABILITY STATEMENT

The data that support the findings of this study are available from the corresponding author upon reasonable request.

ORCID

Zhiming Liu https://orcid.org/0000-0002-8836-8031

REFERENCES

1. Trentini, G.V.: Partially reflecting sheet arrays. IRE Trans. Antenn. Propag. 4(4), 666–671 (1956). https://doi.org/10.1109/tap.1956.1144455
2. Liu, Z., et al.: A wideband Fabry-Pérot antenna with enhanced gain in the high-frequency operating band by adopting a truncated field correcting structure. IEEE Trans. Antenn. Propag. 69(12), 8221–8228 (2021). https://doi.org/10.1109/tap.2021.3090841
3. Gardelli, R., Albani, M., Capolino, F.: Array thinning by using antennas in a Fabry-Pérot cavity for gain enhancement. IEEE Trans. Antenn. Propag. 54(7), 1979–1990 (2006). https://doi.org/10.1109/tap.2006.877172
4. Liu, Z., et al.: Wideband gain enhancement and RCS reduction of Fabry-Pérot antenna using hybrid reflection method. IEEE Trans. Antenn. Propag. 68(9), 6497–6505 (2020). https://doi.org/10.1109/tap.2020.2988949
5. Deng, F., Qi, J.: Shrinking profile of Fabry-Pérot cavity antennas with stratified metasurfaces: accurate equivalent circuit design and broadband

high-gain performance. IEEE Antenn. Wireless Propag. Lett. 19(1), 208–212 (2020). https://doi.org/10.1109/lawp.2019.2958108
6. Sayeed, A.M., Raghavan, V.: Maximizing MIMO capacity in sparse multipath with reconfigurable antenna arrays. IEEE J. Sel. Top. Signal Process. 1(1), 156–166 (2007). https://doi.org/10.1109/jstsp.2007.897057
7. Mehmood, R., Wallace, J.W.: MIMO capacity enhancement using parasitic reconfigurable aperture antennas (RECAPs). IEEE Trans. Antenn. Propag. 60(2), 665–673 (2012). https://doi.org/10.1109/tap.2011.2173445
8. Radavaram, S., Pour, M.: Wideband radiation reconfigurable microstrip patch antenna loaded with two inverted U-slots. IEEE Trans. Antenn. Propag. 67(3), 1501–1508 (2019). https://doi.org/10.1109/tap.2018.2885433
9. Zhang, J., et al.: Automatic AI-driven design of mutual coupling reducing topologies for frequency reconfigurable antenna arrays. IEEE Trans. Antenn. Propag. 69(3), 1831–1836 (2021). https://doi.org/10.1109/tap.2020.3012792
10. Comite, D., et al.: Wideband array-fed Fabry-Pérot cavity antenna for 2-D beam steering. IEEE Trans. Antenn. Propag. 69(2), 784–794 (2021). https://doi.org/10.1109/tap.2020.3008764
11. Debogović, T., Perruisseau-Carrier, J.: Array-fed partially reflective surface antenna with independent scanning and beamwidth dynamic control. IEEE Trans. Antenn. Propag. 62(1), 446–449 (2014). https://doi.org/10.1109/tap.2013.2287018
12. Ji, L., et al.: A reconfigurable partially reflective surface (PRS) antenna for beam steering. IEEE Trans. Antenn. Propag. 63(6), 2387–2395 (2015). https://doi.org/10.1109/tap.2015.2412143
13. Guzman-Quiros, R., et al.: Electronically steerable 1-D Fabry-Pérot leaky-wave antenna employing a tunable high impedance surface. IEEE Trans. Antenn. Propag. 60(11), 5046–5055 (2012). https://doi.org/10.1109/tap.2012.2208089
14. Xie, P., et al.: A dual-polarized two-dimensional beam-steering Fabry-Pérot cavity antenna with a reconfigurable partially reflecting surface. IEEE Antenn. Wireless Propag. Lett. 16, 2370–2374 (2017). https://doi.org/10.1109/lawp.2017.2718567
15. Ourir, A., et al.: Phase-varying metamaterial for compact steerable directive antennas. IET Electron. Lett. 43(9), 493–494 (2007). https://doi.org/10.1049/el:20070298
16. Ratni, B., et al.: Design of phase-modulated metasurfaces for beam steering in Fabry-Pérot cavity antennas. IEEE Antenn. Wireless Propag. Lett. 16, 1401–1404 (2017). https://doi.org/10.1109/lawp.2016.2639463
17. Yang, X., et al.: A radiation pattern reconfigurable Fabry-Pérot antenna based on liquid metal. IEEE Trans. Antenn. Propag. 68(11), 7658–7663 (2020). https://doi.org/10.1109/tap.2020.2993310
18. Dey, A., et al.: Microfluidically reconfigured wideband frequency-tunable liquid-metal monopole antenna. IEEE Trans. Antenn. Propag. 64(6), 2572–2576 (2016). https://doi.org/10.1109/tap.2016.2551358
19. Su, M., et al.: Frequency-reconfigurable liquid metal magnetoelectric dipole antenna. IEEE Antenn. Wireless Propag. Lett. 20(12), 2481–2485 (2021). https://doi.org/10.1109/lawp.2021.3115667
20. Oliner, A.A. In: Johnson, R.C. (ed.) Leaky-wave Antennas. Antenna Engineering Handbook, 3rd ed. McGraw-Hill, New York (1993). ch. 10

How to cite this article: Chen, W., et al.: A two-dimensional beam steering Fabry–Pérot antenna employing a liquid-based reconfigurable metasurface. IET Microw. Antennas Propag. 17(13), 999–1005 (2023). https://doi.org/10.1049/mia2.12420